Clays and Clay Minerals, Vol. 47, No. 2, 119–130, 1999.

"RETROGRADE DIAGENESIS" OF CLAY MINERALS IN THE PRECAMBRIAN FREDA SANDSTONE, WISCONSIN

GENGMEI ZHAO,[1] DONALD R. PEACOR,[1] AND S. DOUGLAS MCDOWELL[2]

[1] Department of Geological Sciences, University of Michigan, Ann Arbor, Michigan 48105-1063
[2] Department of Geological Engineering and Sciences, Michigan Technological University, 1400 Townsend Drive, Houghton, Michigan 49931

Abstract—Siltstones from the Precambrian Freda Formation in Wisconsin have been studied by scanning, scanning-transmission and analytical electron microscopy (SEM, STEM and AEM), and X-ray diffraction (XRD). XRD data for drill core samples show a change from smectite-rich Illite-Smectite (I-S) in shallow samples to illite in deeper samples, implying a transition during burial diagenesis.

Transmission electron microscopy (TEM) observations of shallow samples reveal the presence of three clearly distinguishable kinds of dioctahedral clay minerals: (1) detrital grains of micrometer-sized, mature muscovite; (2) small packets in the matrix consisting of dominant (*Reichweite*) R1 I-S or (3) small packets of illite. The illite and I-S stacks occur separately and have similar textures, with packet thicknesses averaging ~400 Å, within the range of anchizonal illite. Illite and detrital muscovite commonly display strain features typical of the effects of tectonic stress. Void space within I-S or illite packets is inferred to be a strain feature, and to have served as pathways for fluids. Detrital muscovite shows abundant alteration features including (001) boundaries which are continuous with parallel packets of I-S; individual layers commonly show along-layer transitions of muscovite to smectite or I-S. Trioctahedral clays consist primarily of detrital chlorite which commonly shows direct alteration to R1 I-S and smectite, as with detrital muscovite.

Deep samples contain only unaltered, coarse detrital muscovite, and thin packets of illite forming stacks and comprising most of the matrix. The texture of the illite appears to be identical to that of shallow samples, with characteristics such as packet size typical of anchizonal illite. Trioctahedral clays consist almost entirely of detrital grains of chlorite and corrensite. They occur as separate grains with rather constant composition, without signs of alteration.

The data imply that all of the studied rocks have been subjected to a uniform anchizonal grade of metamorphism in which detrital grains were largely unchanged but matrix clays were transformed to packets of illite. The unusually abrupt transition with depth from highly expandable I-S to illite is inferred to actually be the result of subsequent alteration of authigenic illite and detrital chlorite and muscovite to R1 I-S and smectite in shallow rocks. This late overprinting of the anchimetamorphic clay mineral assemblage is inferred to have been locally caused by fluids with temperatures less than those of peak metamorphism. This process, called "retrograde diagenesis", gave rise to a sequence of dioctahedral I-S and illite which mimics classic prograde sequences. Interpretations of such sequences as being prograde, especially in cases of ancient rocks, should be interpreted with caution when high-resolution images of textures are not available.

Key Words—Analytical Electron Microscopy, Chlorite, Freda Formation, Illite, I-S, Muscovite, Retrograde Diagenesis, Scanning Electron Microscopy, Smectite, Transmission Electron Microscopy.

INTRODUCTION

The well-established sequence of evolution of dioctahedral clay minerals which occurs during prograde diagenesis is smectite → random I-S → ordered I-S → $1M_d$ illite → $2M_1$ muscovite. Where this sequence occurs regionally, it usually implies prograde diagenesis, especially if illite increases proportionally with depth of burial (*e.g.*, Hower *et al.*, 1976).

A transition from highly expandable I-S to illite occurs with increasing depth in the Freda Sandstone in Wisconsin, as observed in samples from drill holes (Price and McDowell, 1993). XRD data indicate that R0 I-S with 80% smectite occurs in shallow samples, whereas over a narrow range of 125 m, there is an abrupt but continuous change to clays with <20% expandable layers near the base of the Freda Sandstone. Whereas the progression of changes with depth in this sequence is consistent with typical prograde diagenesis, the abruptness of the change with depth from 80 to 20% expandable layers is not typical, however. The abrupt change is also inconsistent with any plausible rate of reaction involving smectite since the Freda Formation is 1.0–1.1 Ba in age.

Smectite is considered to be a metastable phase by some authors (*e.g.*, Jiang *et al.*, 1994). It commonly forms from materials such as volcanic ash and then generally transforms to illite at low temperatures and in relatively young rocks in an Ostwald-step-rule, prograde sequence where the successive mineral assemblages are of decreasing free energy. By contrast, Price and McDowell (1993) suggested that the clay mineral sequence in the Freda Sandstone in Wisconsin may not have formed under simple prograde conditions, as the abrupt change from >80% to <20% expandable layers requires high geothermal gradients which were in-

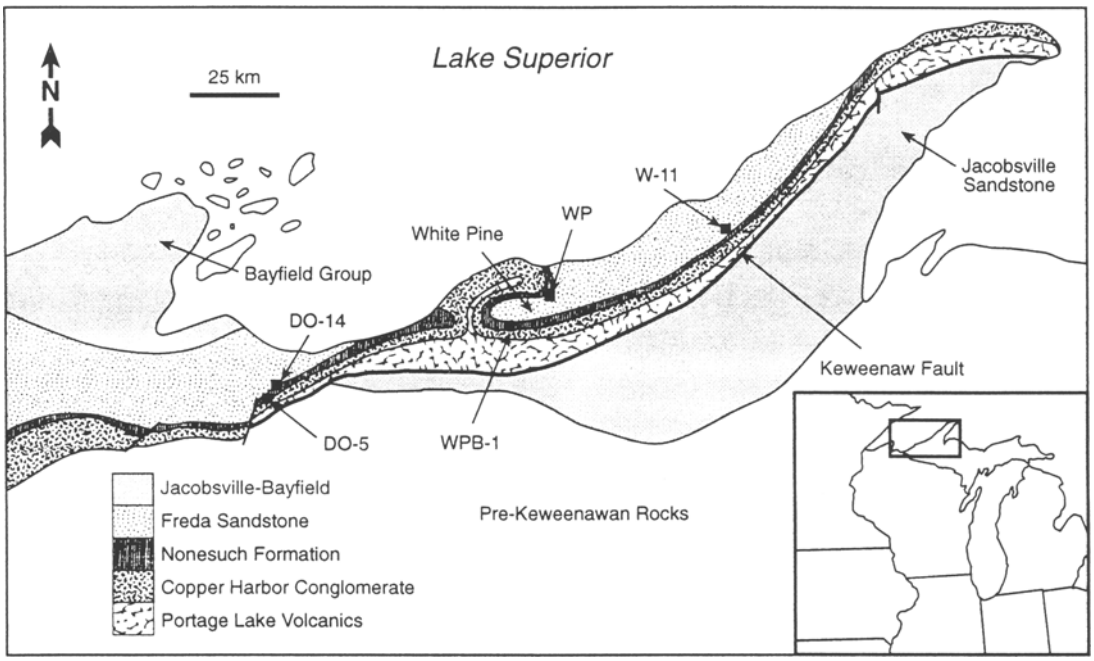

Figure 1. Study area with locations of drill holes DO-5 and DO-14, the source of samples for TEM observations. Modified from Price *et al.* (1993).

ferred to be unlikely. They inferred that fluids may have caused a "back reaction" of higher grade illite to smectite, well after, and at lower temperatures than, the regional prograde event, but this remains an unproven hypothesis.

Similar "retrograde" reactions have recently been postulated by several authors. Jiang *et al.* (1990) observed that mixed-layer I-S formed by replacement of metamorphic illite in Welsh slates at temperatures less than that of peak metamorphism. The reaction is thought to be caused by hydrothermal fluids in association with a major fault system. Nieto *et al.* (1994) described smectite which formed pervasively as an alteration product of high-grade chlorite in the Malaguide Complex of Spain. A well-defined sequence of retrograde reactions occurring on a regional basis was also observed by Nieto (personal communication) in pelitic rocks of San Vicente Cape and the Basque-Cantabrian Basin, Spain, where trioctahedral chlorite was replaced by dioctahedral smectite, and muscovite by I-S.

All of the above studies utilized TEM and AEM to characterize clay minerals directly, in addition to XRD data which were used to characterize minerals in bulk samples and separates. TEM images provide direct characterization of textures of clay mineral assemblages. Such data often permit interpretation of the origins and sequences of formation of minerals, *e.g.*, as in differentiation between prograde and retrograde reactions. The aim of this study was to determine the origin of the smectite-illite trend in the Freda Formation using AEM and TEM.

GEOLOGICAL BACKGROUND

The Freda and Nonesuch Formations are part of the Upper Precambrian Oronto Group, a major rift-filling sequence within the Mid-Continent Rift system (Cannon *et al.*, 1989). As shown in Figure 1, the stratigraphic sequence consists of basal tholeiitic rift basalts (Portage Lake Volcanics), a thick fanglomerate (Copper Harbor Formation), the thin siltstone-shale sequence of the Nonesuch Formation, and the fining-upward cycles of fluvial sandstones, siltstones, and mudstones of the Freda Formation. In the Wisconsin area, the Oronto Group is overlain by the Bayfield Group, a fine-grained clastic sequence formed in a local basin in the waning stages of the Mid-Continent Rift. The rift is thought to have been caused by the Grenville Orogeny (Gordon and Hempton, 1986) or by a mantle plume (Hutchinson *et al.*, 1990; Nicholson and Shirey, 1990) that was active from 1180 to 1086 Ma based on Pb isotope dates (Davis and Sutcliffe, 1985; Davis and Paces, 1990; Palmer and Davis, 1987). The sediments of the Oronto Group represent a rift-filling sequence occurring after 1094 Ma, following a period of intense volcanic/plutonic activity (1098–1094 Ma). The rifting event was brought to a close by a compressional event (1065–1043 Ma; Cannon *et al.*, 1990) which uplifted, folded and faulted the Oronto Group. The compressional event caused a de-

https://doi.org/10.1346/CCMN.1999.0470202 Published online by Cambridge University Press

Table 1. Sample depths and % illite in I-S.

Well	Absolute depth (ft)	Relative depth[1] (m)	% Illite in I-S
DO-14	787	+626	30
DO-14	1775	+335	15
DO-14	2134	+229	15
DO-5	245	+159	50
DO-14	2503	+120	70
DO-5	427	+105	85

[1] Distance above the contact with the Nonesuch Formation.

crease in the width of the rift by ~100 km and developed several local clastic basins (Hedgeman, 1992) including that in which the Bayfield Group was deposited. It is thought to have been related to the Grenville Orogeny to the east.

Thermal modeling of the Oronto Group (Price and McDowell, 1993; Price *et al.,* 1996) suggests that the Nonesuch and lower Freda Formations were buried to depths of 4 km and were subjected to maximum temperatures to 125°C by ~1075 Ma. Erosion of the Freda Sandstone and overlying sediments is assumed to correspond to the compressional event occurring between 1065–1043 Ma (Cannon *et al.,* 1990); the magnitude of erosion must be at least 3 km (Price *et al.,* 1996). The Bayfield Group clastic rocks were most probably deposited during or just after the compressional event, at the time of sudden cooling of sediments from peak metamorphic temperatures to ~70–80°C.

MATERIALS AND METHODS

Sample preparation

Price and McDowell (1993) collected in excess of 150 samples, primarily from drill cores. This material was subsequently made available for this study. The Freda Formation was sampled at five locations (Figure 1), three of which are located in Michigan (W-series) and two in Wisconsin (DO-series). XRD data of Price and McDowell (1993) showed that the clay minerals of the two regions have different expandability. In drill cores from Wisconsin, high-expandability I-S is abundant in shallow samples and low-expandability clay minerals are dominant at greater relative depths, whereas in the Michigan cores, the maximum expandability observed in the Freda Sandstone, for the shallowest samples investigated, was 30%. Six samples from Wisconsin drill cores DO-14 and DO-5 were therefore used in this study for detailed analyses (Table 1).

All samples are red to brownish in color and range in texture from siltstones to very fine-grained sandstones. When some samples were placed in contact with water, the surfaces expanded and spalled away due to the expansion of smectite interlayers. To prevent collapse of the expandable layers during sample preparation and observation, the samples were treated with LR White resin (Kim *et al.,* 1995).

Methods

A Philips diffractometer with graphite monochromator and CuKα radiation (35 kV, 15 mA) was used to obtain XRD data of bulk rock samples and the <2 μm size fraction to verify that the samples typified the observations of Price and McDowell (1993). Polished thin sections were made using sticky-wax as an adhesive. The impregnated sections were oriented normal to bedding. TEM samples were then prepared by attaching aluminum washers with diameters of 3 mm to selected areas, which were then removed for ion milling. SEM observations were carried out with a Hitachi S-570 SEM which includes a back-scattered electron (BSE) detector and Kevex Quantum energy dispersive spectrum (EDS) analysis system. Areas identified as typical by SEM were then studied with a Philips CM12 STEM fitted with a Kevex Quantum EDS system and operated at an accelerating voltage of 120 kV and a beam current of 10 μA. Most images were obtained at 100,000× magnification with an objective aperture of 30 μm. Selected area electron diffraction (SAED) patterns were obtained with a camera length of 770 mm. EDS data were obtained in scanning mode over 300 × 300 Å areas and processed using k-factors as defined by Jiang *et al.* (1994). AEM analyses were obtained only from grains which were first characterized by TEM techniques. Clay minerals were imaged and characterized using the techniques of Guthrie and Veblen (1989, 1990), Veblen *et al.* (1990), and Jiang *et al.* (1990). Mineral identification was based on collective data on textures, spacings of lattice fringes, SAED patterns, and AEM analyses.

RESULTS

XRD observations

XRD patterns were consistent with the results of Price and McDowell (1993), and the reader should refer to their results for examples and detailed interpretation of the XRD patterns of the clay minerals. The abundant minerals in shallower samples of the Freda Sandstone are feldspars, quartz, hematite, kaolinite, illite, chlorite, and R1 I-S, whereas deeper samples are similar except that I-S is absent and corrensite is relatively abundant. The proportion of smectite in I-S is large in shallow samples and decreases dramatically over a depth interval of ~125 m, as shown by data in Table 1.

SEM observations

Figure 2 includes four SEM images illustrating typical textures. Figure 2a and 2b is from the two shallowest samples (DO-14-787 and DO-14-1775) and Figure 2c and 2d is from the deepest ones (DO-14-2503 and DO-5-427). Large (>10 mm) subangular grains of detrital origin dominate these samples. EDS analysis showed that most are quartz or K-feldspar.

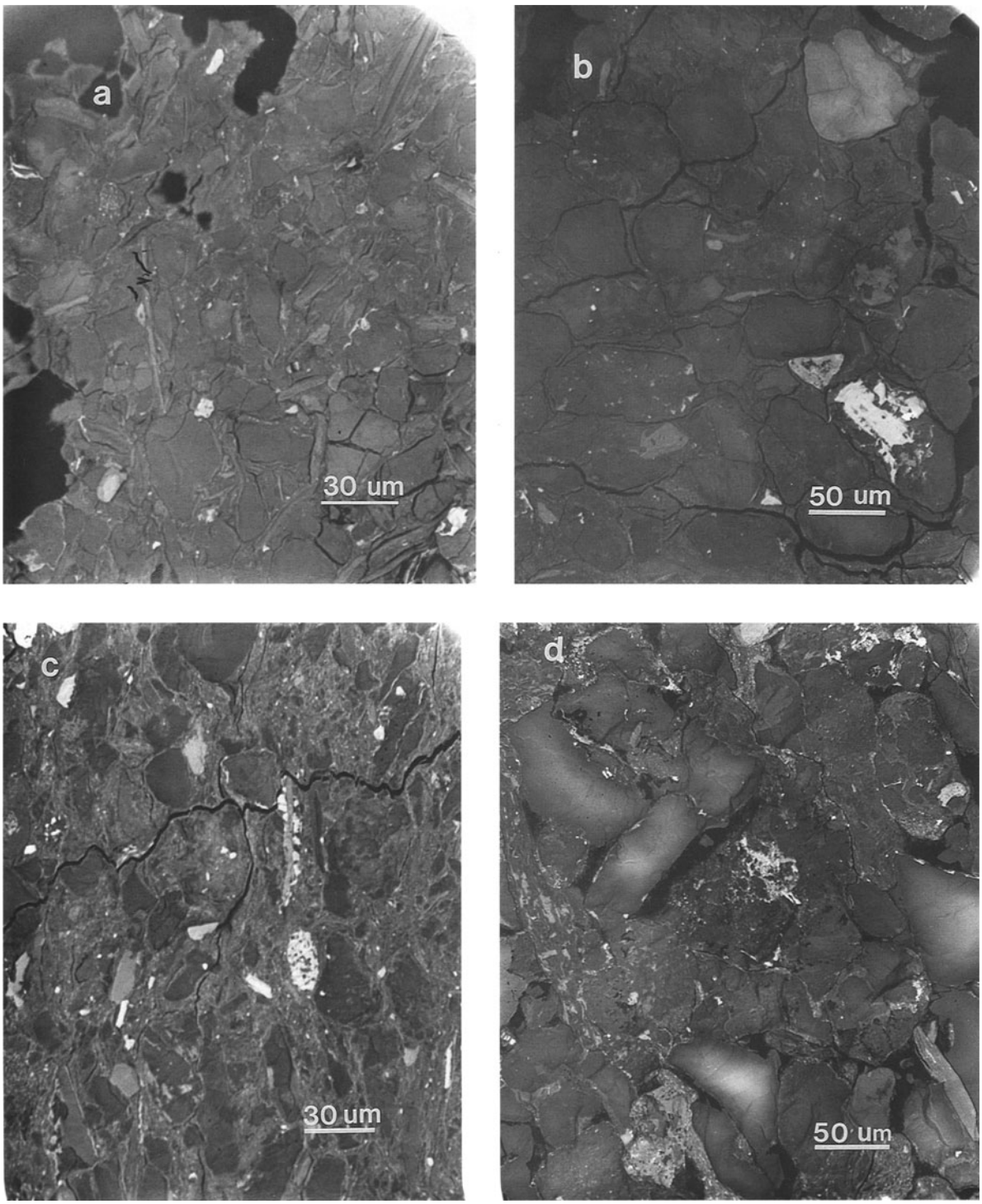

Figure 2. Low magnification back-scattered electron SEM images of samples prepared for TEM observation by ion milling. Large detrital grains consist largely of quartz, feldspar, chlorite and muscovite. The "matrix" clay minerals occur as ill-defined areas between detrital grains and commonly include small grains of hematite with bright contrast. Shallowest two samples: (a) sample DO-14-787; (b) sample DO-14-1775; deepest two samples: (c) sample DO-14-2503; (d) sample DO-5-427.

https://doi.org/10.1346/CCMN.1999.0470202 Published online by Cambridge University Press

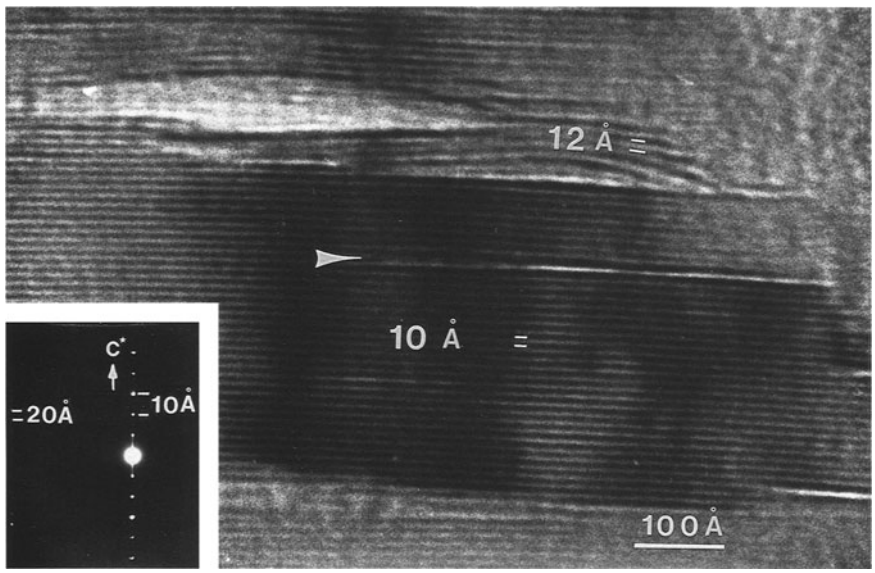

Figure 3. Lattice fringe image showing a portion of a detrital muscovite grain consisting of straight 10-Å fringes, sample DO-14-787. In the upper part of the figure, 10-Å muscovite fringes change laterally to the right to 12-Å, curved fringes of smectite. One lens-shaped void is occupied by vaguely defined smectite fringes. The SAED pattern indicates dominant $2M_1$ muscovite, with streaking along c^* as consistent with the presence of layers of variable spacing. The arrow points to a layer termination within muscovite. The terminated muscovite layer is represented by an enlarged spacing to the right, unlike dislocation-like features, and as observed in grains affected by alteration.

Some large elongated, detrital grains with intermediate contrast gave EDS spectra which are qualitatively consistent with chlorite and muscovite. Fine-grained hematite with bright contrast is ubiquitous. The space between detrital grains (the matrix) is occupied by material which displays relatively homogeneous contrast, but which, at high magnification, appears to be somewhat mottled, with some sub-micrometer sized component grains displaying the bright contrast typical of hematite. EDS analyses of the fine-grained matrix are quite variable, but commonly have peaks consistent primarily with minor amounts of iron oxide (presumably hematite) and variable proportions of the trioctahedral and dioctahedral clay minerals later identified by TEM. As shown in Figure 2b, cracks commonly occur at the boundaries of detrital grains and matrix, especially in shallow samples, as consistent with dehydration of smectite interlayers in the vacuums of the ion mill or SEM.

TEM data for the four shallow samples (DO-14-787, DO-14-1775, DO-14-2134, DO-5-245)

TEM observations show that shallow samples contain five kinds of phyllosilicate, consisting of: (1) large, detrital grains of partially altered muscovite, alteration products consisting of I-S and smectite; (2) detrital, partially altered grains of trioctahedral phyllosilicates, primarily chlorite; (3) packets of authigenic illite in the matrix; (4) packets of I-S with dominant R1 ordering in the matrix; and (5) smectite, occurring primarily as an alteration product of detrital phyllosilicates. Each kind of phyllosilicate is described in the following sections.

Detrital muscovite. Detrital muscovite occurs as grains which are typically at least hundreds of layers thick, a small portion of one being shown in Figure 3. Most lattice fringes are typically straight with homogeneous contrast, and free of layer terminations. SAED patterns are consistent with $2M_1$ polytypism, and AEM-determined compositions approach those of ideal muscovite.

Detrital muscovite commonly shows abundant alteration features, however, as illustrated in the upper portion of Figure 3. Straight 10-Å mica fringes are seen to change laterally from left to right into layers with 11–12-Å spacings. The layers are curved and have irregular contrast, as is typical of smectite. Void space occurs locally where layers appear to be deformed. In addition, in the region where such apparent alteration features occur, mica layers are commonly observed to terminate at sites where contrast changes radically (arrow in Figure 3). Unlike typical layer terminations however, for which associated fringe spacings are 10 Å, the layer which appears as a continuation of the terminated fringe has a spacing of >10 Å. Such features have the general appearance of "along-layer" alteration, rather than of dislocations formed during crystal growth. The muscovite analysis given in Table 2 is from an area showing such alteration features. The smaller Al and K contents relative to mature muscovite imply the presence of smectite- or

https://doi.org/10.1346/CCMN.1999.0470202 Published online by Cambridge University Press

Table 2. Representative structure formulae derived from AEM analysis of clay minerals[1,2].

	Muscovite[3]	Illite[3]	I-S[3]	Smectite[3]	Corrensite	Chlorite[3]
Si	6.65	6.98	7.06	7.19	7.32	6.29
Al (IV)	1.36	1.02	0.94	0.81	0.68	1.71
Al (VI)	3.27	2.90	3.10	2.96	5.63	3.05
Fe^{2+}	0.70	0.83	0.41	0.72	0.69	3.37
Mg	0.18	0.75	0.82	0.35	2.99	4.66
Ti	0.05	0.00	0.00	0.00	0.00	0.00
Mn	0.00	0.01	0.00	0.11	0.00	0.15
Na	0.07	0.00	0.39	0.56	0.24	0.00
K	1.34	0.82	0.46	0.31	0.18	0.00
Ca	0.10	0.17	0.17	0.23	0.00	0.11
Total cations	13.70	13.47	13.35	13.24	17.72	19.34

[1] Each formula for muscovite, illite, I-S and smectite is normalized to a total of 12 cations in the tetrahedral and octahedral sites.

[2] Each formula for corrensite and chlorite is normalized on the basis of 28 O atoms.

[3] Formulae differ from ideal compositions due to inclusion of some relict muscovite or illite in I-S and smectite, and secondary smectite layers in muscovite, illite, and chlorite (see text for description).

I-S-like material. Analyses of the smectite gave higher than normal interlayer K, Na, and Ca contents, but this is consistent with the inclusion of some mica or illite-like layers within the areas of analysis of these thin packets.

The curvature of smectite-like layers shown in Figure 3 defines lens-shaped voids. These are abundant wherever smectite-like fringes appear to be laterally continuous with adjacent mica fringes, or are parallel to adjacent mica fringes. The voids commonly appear to be occupied by vaguely-defined fringes with spacings of ~12 Å, as consistent with infilling by smectite, but are so small and ill-defined as to prevent complete characterization.

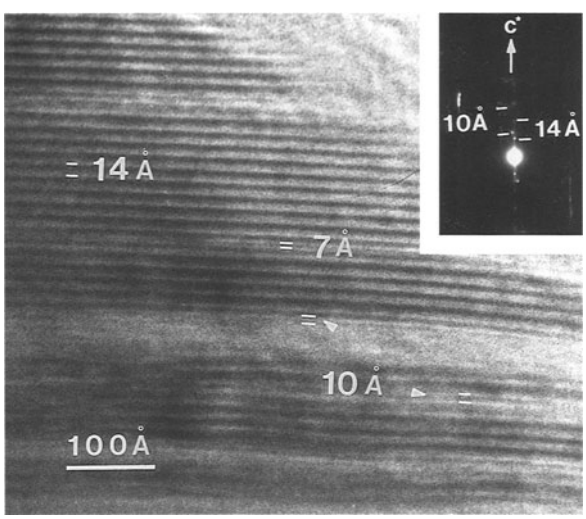

Figure 4. Lattice fringe image of a detrital trioctahedral clay mineral grain from sample DO-14-2134, illustrating mixed layering of 14-Å chlorite, 7-Å berthierine and 10-Å smectite (arrow). 10-Å layers have less contrast compared to the others. The SAED pattern shows discrete reflections corresponding to 14-Å chlorite and 10-Å smectite, with streaking as consistent with random mixed-layering.

Detrital trioctahedral phyllosilicates. Trioctahedral phyllosilicates occur only rarely in the matrix, but are common as large detrital grains which are almost exclusively chlorite with abundant deformation and alteration features. Figure 4 shows a small portion of a crystal consisting largely of chlorite, with shape and size typical of detrital grains when viewed at low resolution (not shown). Fringes are typically sharply defined with 14-Å spacings. Some 7-Å berthierine-like layers occur, as typical of relict trioctahedral material formed at lower grades in a prograde sequence (*e.g.,* Ahn and Peacor, 1985). In the lower part of Figure 4, however, fringes with ~10-Å spacing occur on the right side of the image. In some cases they change laterally to 14-Å layers. Where more than one such layer occurs, contrast is commonly so poorly defined that the fringes are barely visible. Nevertheless, it is apparent that such features reflect a transformation between chlorite and material with 10-Å fringe spacings.

Figure 5 shows a large packet of detrital chlorite with straight 14-Å fringes with homogeneous contrast bordered by material with subparallel layers and 10–11-Å spacings. Few defects occur within this crystal; however, along its upper boundary, 14-Å fringes change laterally to fringes having spacings of 10–11-Å. There is a one-to-one relationship, implying that individual 10–11-Å layers were replaced by 14-Å layers (marked with arrows), or *vice versa.* The compositions and structures of such individual layers can not be directly determined. However, the transitional 10–11-Å fringes correspond to the lowest layer of a thick packet of subparallel 10–11-Å layers. Some of those fringes show typical 21-Å two-layer periodicity and curved layers as consistent with R1 I-S. With a change of focus conditions (not shown in this picture), the 10–11-Å fringes displayed 21-Å periodicity. The AEM data of such extended areas are consistent with R1 I-S. In addition, two parallel sets of 001 reflections oc-

https://doi.org/10.1346/CCMN.1999.0470202 Published online by Cambridge University Press

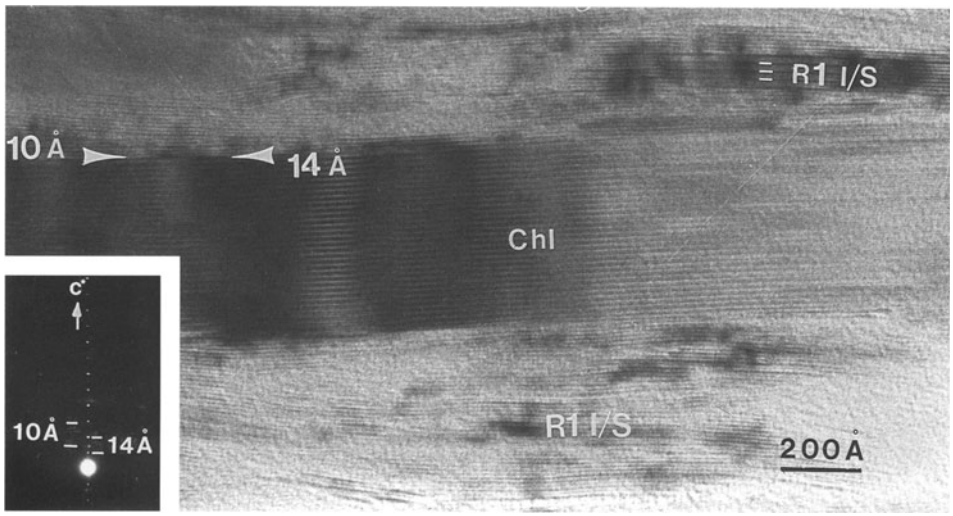

Figure 5. TEM image from sample DO-14-1775 showing the relationship between detrital chlorite and I-S. The I-S occurs as stacks with layers parallel to subparallel with respect to chlorite layers. The region between the arrows illustrates layers (which appear to be coherent with respect to the chlorite packet) which change laterally from 14-Å to 10-Å. Corresponding electron diffraction patterns show strong and sharp 14-Å reflections and weak 10-Å reflections.

curred in the SAED pattern (inset, Figure 5). The sharp and intense reflections with 14-Å periodicity were derived from the chlorite whereas the reflections with 10–11-Å periodicity were faint and diffuse as typical of smectite or I-S.

Smectite. Smectite ubiquitously occurs as packets consisting of a few layers (*e.g.,* Figure 3) only in close association with I-S, and is inferred to be an alteration product of detrital muscovite or chlorite, as described above. It was identified by its wavy and anastomosing fringes, common layer terminations, fringe spacing of >10 Å, diffuse and weak reflections in SAED patterns, and AEM analyses.

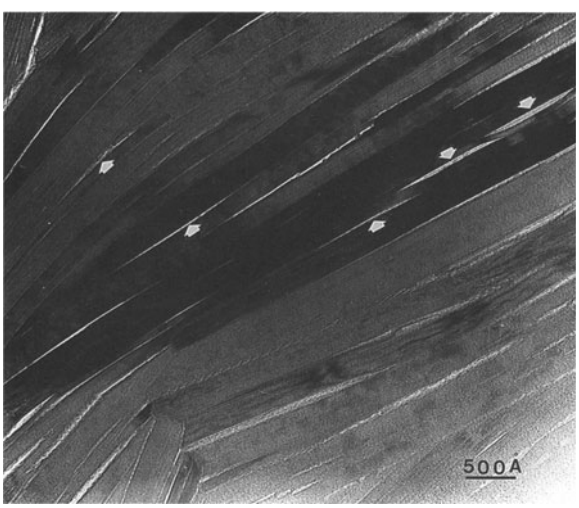

Figure 6. Low magnification TEM image from sample DO-5-245 showing matrix illite consisting of packets which are ~500 Å thick (typical of anchizone). Note the curved packets in the upper left and the broken and healed packets in the lower area. Deformation has produced numerous void spaces (marked with arrows).

Matrix illite. Figure 6 shows the first of two kinds of matrix dioctahedral clay minerals, which is less abundant than the R1 I-S described above. It consists of subparallel, thin (<50 layers) packets of illite. It was characterized in part by AEM analyses which exhibit significantly less Al in tetrahedral sites, and K contents in the interlayers, as compared to muscovite. SAED patterns always show relatively sharp and strong 00*l* reflections and diffuse, ill-defined non-00*l* reflections typical of $1M_d$ stacking.

The individual packets of illite are 100–500 Å in thickness, as typical of illite of the anchizone and in marked contrast to the I-S from the same samples (see below). The packets of layers in the upper left of the figure are curved, defining an anticline-like structure, whereas the contiguous packets in the lower area are straight, but have sharp terminations defined by layers at high angles. They appear to have been ruptured at sites of maximum curvature. Such deformation features are abundant in the illite.

Matrix I-S. Figure 7a shows packets defined by lattice fringes with contrast having two-layer periodicity corresponding primarily to R1 I-S. The image in Figure 7a was obtained with focus conditions as defined by Guthrie and Veblen (1989, 1990) which optimize such contrast between illite-like and smectite-like interlayers. Periodicity is 21 Å, as observed by Dong and Peacor (1996) to be typical of R1 I-S in samples treated by LR White resin, rather than the larger values (*e.g.,* 24 Å) typical of the sum of 10-Å illite-like and

https://doi.org/10.1346/CCMN.1999.0470202 Published online by Cambridge University Press

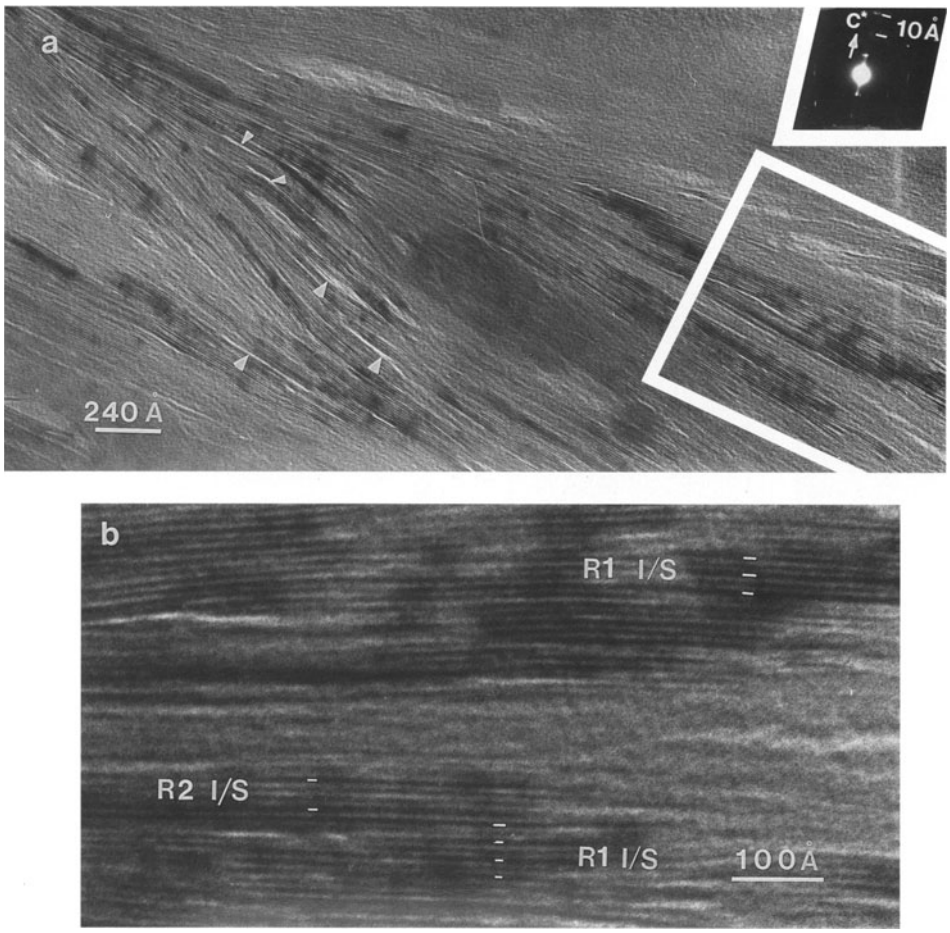

Figure 7. (a) Low magnification TEM image illustrating a stack of R1 I-S layers in the matrix of sample DO-14-787. Void spaces are abundant (marked with arrows). (b) An enlarged area of part (a) displaying alternating darker and lighter fringes as consistent with dominant R1 I-S with locally occurring R2 I-S.

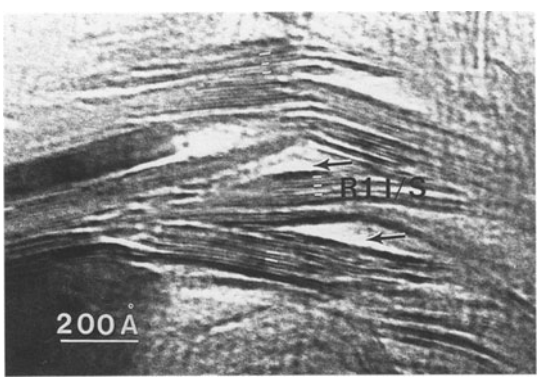

Figure 8. TEM lattice fringe image from sample DO-5-245 displaying kinking of I-S packets. Triangular void spaces (marked with arrows) were generated by layer deformation, as consistent with tectonically-induced stress.

fully expanded smectite-like interlayers. Identification was also confirmed by AEM analyses (Table 1) and SAED patterns which have non-00*l* reflections which are non-periodic, diffuse, and weak.

I-S typically occurs as subparallel packets whose thicknesses and texture commonly appear to be identical to those of illite. Void spaces (marked with arrows) are abundant and, as discussed below, may be significant as conduits for fluid transport. Figure 7b is an enlarged part of Figure 7a, illustrating alternate bright and dark fringes corresponding to smectite-like and illite-like layers with 21-Å periodicity typical of R1 I-S. Some layers, however, display three-layer periodicity which corresponds to R2 I-S.

Figure 8 is a lattice fringe image of several I-S packets with typical R1 periodicities, layer terminations, and wavy or curved fringes. Layers are sharply kinked as typical of metamorphic strain features (Jiang *et al.*, 1990). Triangular void spaces are directly associated with kinked layers. Figure 9a shows material which has the appearance of typical illite; however, the

https://doi.org/10.1346/CCMN.1999.0470202 Published online by Cambridge University Press

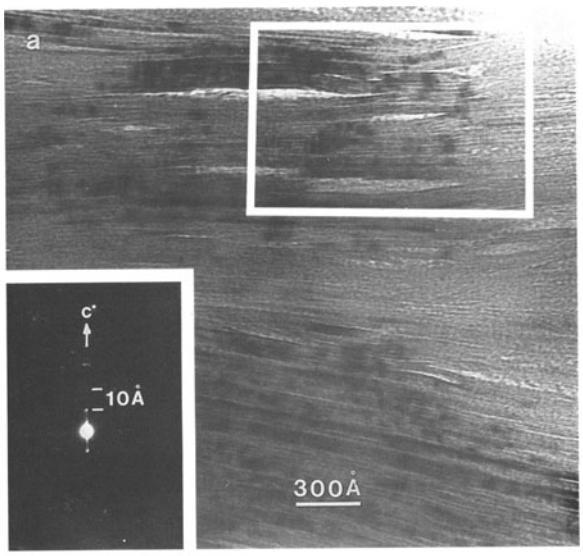

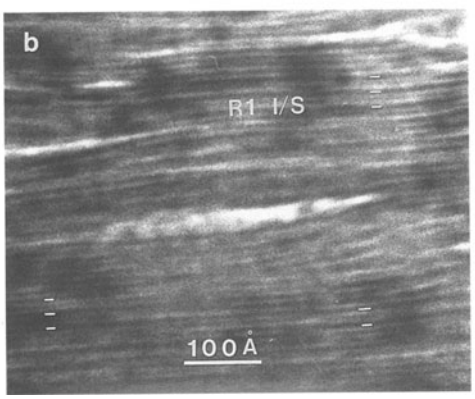

Figure 9. (a) TEM image from the matrix of sample DO-5-245 consisting largely of R1 I-S. Curved fringes, layer terminations, and void spaces are common. The corresponding SAED patterns show diffuseness along c^*. (b) An enlarged area of part (a) showing the two-layer periodicity as indicated by fringe contrast corresponding to R1 I-S.

curvature of layers, dominant two-layer periodicity, layer terminations, and relatively large fringe spacing show that it is R1 I-S occurring as a thick sequence of subparallel to parallel layers. Figure 9b is an enlarged area of Figure 9a, with contrast in fringes indicating dominant I-S periodicity, but with local disorder. Illite may also occur as such extended sequences of subparallel packets, but with sharper definition of boundaries of individual packets (*e.g.,* Figure 6).

TEM data for the two deeper samples (DO-14-2503, DO-5-427)

Matrix dioctahedral clay minerals. The dioctahedral clay minerals in the deeper samples are quite different from those in the shallower samples in that only illite is observed as a dioctahedral component of the matrix; *i.e.,* no I-S was observed, as consistent with XRD observations. The textures are similar to those of the matrix illite of shallow samples as exemplified by Figure 6; *i.e.,* the illite is composed of stacks of subparallel thin packets, with a mean thickness of ~400 Å. Common strain features are typical of a metamorphic environment and consist of features such as bent, kinked, broken, or healed layers.

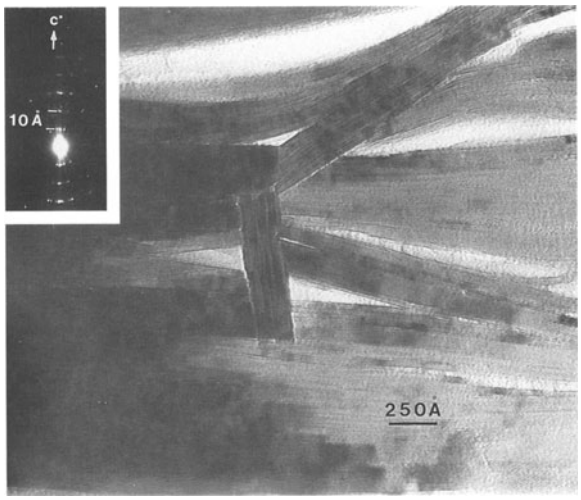

Figure 10. TEM image of sample DO-5-427 showing packets of illite which have been deformed, creating pore space.

Detrital clay minerals. The large detrital phyllosilicate grains are comprised almost exclusively of relatively homogeneous muscovite, corrensite, or chlorite. Alteration-like features were observed only rarely. Deformation-induced features include kinked and bent layers, with abundant, closely associated void spaces as illustrated by Figure 10.

Trioctahedral clay minerals in the deeper samples occur only as detrital grains, as is the case for shallow samples. By contrast with shallow samples, there are two types of detrital grains which consist principally either of chlorite or corrensite layers, the former being much more common. AEM data show that different chlorite grains have similar compositions, and that the compositions are similar to those of shallow samples. Although mixed-layering occurs, no alteration to dioctahedral I-S was detected. Figure 11 shows relations for a crystal composed dominantly of chlorite, but which also contains complex mixed-layering. Three kinds of layers exist: 14-Å chlorite layers (marked with black arrows), 7-Å berthierine layers, and 10-Å smectite-like layers (marked with white arrows). The latter are consistent with local corrensite-like units, *i.e.,* trioctahedral smectite.

DISCUSSION

Interpretation of microscopic observations

The illite that occurs in the matrix of deeper samples has a mean packet thickness of ~400 Å. It is well

https://doi.org/10.1346/CCMN.1999.0470202 Published online by Cambridge University Press

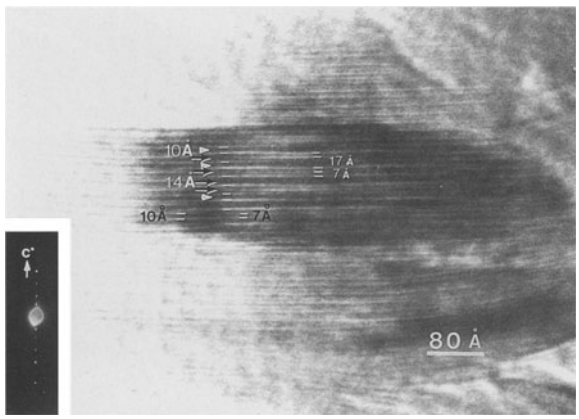

Figure 11. TEM image of sample DO-14-2503 showing a detrital grain consisting largely of corrensite. The small region of the grain which is shown consists of intercalated 7-Å, 10-Å and 14-Å layers.

established that the thickness of illite crystallites increases regularly in a prograde sequence, a value of 400 Å corresponding to anchizonal conditions (*e.g.,* Arkai *et al.,* 1996; Jiang *et al.,* 1997). By contrast, crystal thicknesses of ~100 Å are typical of illite in shales of the Gulf Coast, occurring at depths greater than that of the smectite-to-illite transition (Merriman, personal communication). Furthermore, the illite has the collective characteristics of illite formed under anchizonal conditions, including $1M_d$ polytypism, composition intermediate to those of smectite and muscovite, relatively low density of layer terminations, and lack of smectite-like interlayers, the latter two characteristics being diagnostic of grade. A down-core transition of I-S, as suggested by XRD data, would require that the resulting illite, which presumably is the initial reaction product of I-S, has the characteristics of diagenetic illite, as typically represented, *e.g.,* by that in Gulf Coast sediments. The anchizonal grade of illite is further implied by the presence of abundant strain features in the illite, including bent, kinked, and ruptured packets, with resultant production of pore space. Such features are atypical of the burial diagenetic environment, including the range of grade over which smectite transforms to illite. They are typical of the anchizonal environment, however (*e.g.,* Jiang *et al.,* 1997).

The same kind of illite which forms the bulk of the matrix in deeper samples also occurs as a major component in the matrix of the shallow four samples, implying that the shallow section has attained the same grade of metamorphism as the deeper section. However, the shallow samples are replete with examples of hydrothermal alteration as represented by altered detrital muscovite and chlorite, and the occurrence of stacks of R1 I-S in the matrix. The latter generally is observed in portions of samples separate from those in which illite occurs, but has the same crystallite thicknesses, form, and strain features as the illite which is typical of anchizonal grade, implying that it is anchizonal-grade illite which has been locally replaced by I-S, perhaps in those portions of samples with enhanced permeability. Similar selective replacement relations were observed by Jiang *et al.* (1990) for illite of shale which was partially replaced by I-S by the action of hydrothermal fluids.

Detrital chlorite and muscovite of shallow samples were frequently observed to be bordered by thin stacks of parallel layers consisting primarily of R1 I-S, but also of smectite. Outer layers of such detrital crystals were commonly observed to have lateral transitions into R1 I-S. The chlorite portions of such partially transformed layers appeared to be coherent with respect to the adjacent parallel chlorite layers, and the R1 I-S portions appeared to be coherent with respect to adjacent parallel layers of R1 I-S. Such relations illustrate "along-layer" alteration of chlorite or muscovite to R1 I-S or smectite. Crystals which display alteration at boundaries also commonly display layer terminations with very different appearances compared to those of common dislocations (layer terminations). Muscovite or chlorite layers are observed to transform laterally to fringes with an inordinately large interlayer spacing which give strong contrast in TEM lattice fringe images, and which continue to the borders of crystals. Such features suggest "along-layer" alteration.

The detrital muscovite and, especially, the authigenic illite commonly display curved layers and packets with sharp terminations which have appearances similar to strain features observed in tectonically-deformed illite (*e.g.,* Merriman *et al.,* 1995; Jiang *et al.,* 1997). This similarity, coupled with the consistency of the metamorphic grade, suggests that the observed microstructural deformation features are due to tectonic stress. Flexing of layers produces layer or packet separation, resulting in void space (Figure 3). In addition, where severe deformation was observed, including kinking, fracturing, and annealing of packets (Figures 6 and 10), void spaces with triangular shape were created.

Genesis of clay minerals

The collective data imply that illite occurring in the matrix was formed before or during deformation. That is entirely consistent with thermal modeling of the rift sediments (Price and McDowell, 1993; Price *et al.,* 1996). Authigenic minerals are inferred to have first formed during gradual burial (1090–1070 Ma) at temperatures up to ~100°C. Deformation occurred during the later compressional event (after 1070 Ma) when the sediments were uplifted ~2 km and relatively rapidly cooled to temperatures below 80°C. The anchizonal illite is inferred to have formed and been deformed during this event. Sediments in the shallow

portion of the sequence were subsequently altered by hydrothermal fluids. Regional fluid-rock interactions which have been localized within specific stratigraphic horizons have been documented by others (*e.g.,* Evans and Battles, 1997; Ziegler and Longstaffe, 1997). This sequence of events is consistent with the observation that replacement of illite by I-S appears to be much more prevalent where deformation features were observed. Tectonic-stress induced strain in crystals promotes their reactivity, whereas the voids produced by deformation provide conduits for fluids promoting reactions (Jiang *et al.,* 1990).

Similar observations were documented by Jiang *et al.* (1990) for alteration of anchizonal illite to R1 I-S in samples near a major fault zone which presumably served as a local source of fluids. The low grade of those samples contrasted sharply with the regional grade of metamorphism. Nieto *et al.* (1994) observed alteration of trioctahedral chlorite to dioctahedral I-S on a regional basis, implying that such alteration occurred as a major geologic event subsequent to earlier anchizonal metamorphism. Similarly, Nieto (personal communication) has observed replacement of illite by I-S in sediments of the Basque-Cantabrian Basin, and of chlorite and muscovite by smectite in the San Vicente Sequence, Spain. The latter examples of regional-scale alteration to phases typical of lower grades were apparently due to enhanced fluid activity associated with tectonic deformation.

We therefore conclude that "retrograde diagenesis" of clay minerals (Nieto *et al.,* 1994) may be induced by hydrothermal fluids which postdate and overprint the effects of the lowest grades of metamorphism. Retrograde reactions involve dissolution and crystallization through hydration, and water must play a significant role. Because such reactions occur at low temperatures where "solid state" reaction rates are vanishingly small, fluids are essential as agents of dissolution and neocrystallization, as components of reaction products, and as the medium for transport of reactants and products. The rocks of the nearby Precambrian Nonesuch Formation were shown to have achieved a very low grade of metamorphism (anchizonal) during the Grenville Orogeny, but organic material and clay minerals remained unchanged for ~1 Ga years since that time (Li *et al.,* 1995). We infer that such low-grade "retrograde diagenesis" will occur only during regional low-grade metamorphic events which may induce enhanced fluid activity over the relatively short time intervals corresponding to tectonic activity.

This is in agreement with thermal modeling results of Price and McDowell (1993). Their study implies that the Freda-Nonesuch sediments cooled relatively rapidly after 1070 Ma, from >100°C to <80°C as the area was uplifted during late stage compression. Once uplifted, the sediments cooled very slowly over the last billion years, allowing the organic materials and low-grade clay minerals to be preserved. The compressional event could have easily led to back reaction of the layer silicates, as strain energy was added to the system through deformation. The combination of strain energy and mixing with low temperature brines presumably in equilibrium with smectite or I-S but not illite, would promote back reaction.

Geological implications

At the time of uplift and deformation of the southern flank of the Mid-Continent Rift in northern Michigan and Wisconsin, local sedimentary basins developed both to the northwest and southeast of the study area. The basin to the north, centered on the Bayfield Peninsula northwest of Ashland, Wisconsin, contains a clastic section with very clean, fine-grained sandstones and siltstones in the Bayfield Group that could easily have originated in part from erosion of the Freda Formation. These rocks overlie the Freda Formation unconformably both on land and in seismic profiles taken in Lake Superior (Cannon *et al.,* 1989). Although it is not known whether the Bayfield Group extended into the study area and was subsequently removed by erosion, it is likely that the groundwater system associated with the development of the basin was present in the study area. The relatively porous Freda Formation would have been the site of mixing of the low temperature, low salinity groundwater system and the higher temperature diagenetic/metamorphic brines originally present during prograde alteration to illite. This cooler fluid could have overprinted the earlier prograde alteration, producing smectite and highly expandable I-S as alteration products of preexisting illite in the Freda Formation immediately above the relatively more impermeable Nonesuch Formation. The result was a very abrupt transition over a 125 m depth interval, from smectite and I-S with >80% expandability to illite near the base of the Freda Formation. Further east in Michigan, away from the influence of this superimposed hydrogeologic system, no retrograde alteration is observed, and a transition from clay, with only 30% expandability, to illite occurs gradually over a depth range of >500 m, as observed in undisturbed fossil diagenetic systems.

ACKNOWLEDGMENTS

We thank G. Li, H. Dong, and C. Henderson for helping with the sample preparation and TEM procedures. We are grateful to B. A. van der Pluijm, R. Schegg, and an anonymous reviewer for their reviews and suggestions for improvement in the manuscript. This work was supported by NSF grant EAR-94-18108 to D.R. Peacor. The STEM used in this study was acquired under NSF grant ER-87-08276 and the SEM under NSF grant BSR-83-14092.

REFERENCES

Ahn, J.H. and Peacor, D.R. (1985) Transmission electron microscopic study of diagenetic chlorite in Gulf Coast argillaceous sediments. *Clays and Clay Minerals,* **33,** 228–236.

Arkai, P., Merriman, R.J., Roberts, B., Peacor, D.R., and Toth, M. (1996) Crystallinity, crystallite size and lattice strain of illite-muscovite and chlorite: Comparison of XRD and TEM data for diagenetic to epizonal pelites. *European Journal of Mineralogy,* **8,** 1119–1137.

Cannon, W.F., Green, A.G., Hutchinson, D.R., Lee, M., Milkereit, B., Behrendt, J.C., Halls, H.C., Green, J.C., Dickas, A.B., Morey, G.B., Sutcliffe, R., and Spencer, C. (1989) The North American Midcontinent rift beneath Lake Superior from GLIMPCE seismic reflection profiling. *Tectonics,* **8,** 305–332.

Cannon, W.F., Peterman, Z.E., and Sims, P.K. (1990) Structural and isotopic evidence for middle Proterozoic thrust faulting of Archean and early Proterozoic rocks near the Gogebic range, Michigan and Wisconsin. *Institute on Lake Superior Geology Proceedings,* **36,** 11–113.

Davis, D.W. and Sutcliffe, R.H. (1985) U-Pb ages from the Nipigon Plate and Northern Lake Superior. *Geological Society of America Bulletin,* **96,** 1572–1579.

Davis, D.W. and Paces, J.B. (1990) Time resolution of geologic events on the Keweenaw Peninsula and implications for development of the Midcontinent Rift system. *Earth and Planetary Science Letters,* **97,** 54–64.

Dong, H. and Peacor, D.R. (1996) TEM observations of coherent stacking relations in smectite, I/S and illite of shales: Evidence for MacEwan crystallites and dominance of $2M_1$ polytypism. *Clays and Clay Minerals,* **44,** 257–275.

Evans, M.A. and Battles, D.A. (1997) Regional syn-orogenic fluid migration in the central Appalachians: Fluid geochemistry and fluid migration pathways. In *Contributions to the Second International Conference on Fluid Evolution, Migration and Interaction in Sedimentary Basins and Orogenic Belts, Belfast, Northern Ireland,* J.P. Hendry, P.F. Carey, J. Parnell, A.H. Ruffell, and R.H. Worden, eds., 85–88.

Gordon, M.B. and Hempton, M.R. (1986) Collision induced rifting: The Grenville orogeny and Keweenawan rift of North America. *Tectonophysics,* **127,** 1–25.

Guthrie, G.D., Jr. and Veblen, D.R. (1989) High-resolution transmission electron microscopy of mixed-layer illite/smectite: Computer simulations. *Clays and Clay Minerals,* **37,** 1–11.

Guthrie, G.D., Jr. and Veblen, D.R. (1990) Interpreting one-dimensional high-resolution transmission electron micrographs of sheet silicates by computer simulation. *American Mineralogist,* **75,** 276–288.

Hedgman, C.A. (1992) Provenance and tectonic setting of the Jacobsville Sandstone, from Ironwood to Keweenaw Bay, Michigan. M.S. thesis, University of Cincinnati, Cincinnati, Ohio, 158 pp.

Hower, J., Eslinger, E.V., Hower, M.E., and Perry, E.A. (1976) Mechanism of burial metamorphism of argillaceous sediments: Mineralogical and chemical evidence. *Geological Society of America Bulletin,* **87,** 725–737.

Hutchinson, D.E., White, R.S., Cannon, W.F., and Schultz, K.J. (1990) Keweenawan hot spot: Geophysical evidence for a 1.1 Ga mantle plume beneath the Midcontinent rift system. *Journal of Geophysical Research,* **95,** 10869–10884.

Jiang, W.T., Peacor, D.R., Merriman, R.J., and Roberts, B. (1990) Transmission and analytical electron microscopic study of mixed-layer illite/smectite formed as an apparent replacement product of diagenetic illite. *Clays and Clay Minerals,* **38,** 449–468.

Jiang, W.T., Peacor, D.R., and Essene, E.J. (1994) Clay minerals in the MacAdams sandstone, California: Implications for substitution of H_3O^+ and H_2O and metastability of illite. *Clays and Clay Minerals,* **42,** 35–45.

Jiang, W.T., Peacor, D.R., Arkai, P., Toth, M., and Kim, J.W. (1997) TEM and XRD determination of crystallite size and lattice strain as a function of illite crystallinity in pelitic rocks. *Journal of Metamorphic Geology,* **15,** 267–281.

Kim, J.W., Peacor, D.R., Tessier, D., and Elsass, F. (1995) A technique for maintaining texture and permanent expansion of smectite interlayers for TEM observations. *Clays and Clay Minerals,* **43,** 51–57.

Li, G., Mauk, J.L., and Peacor, D.R. (1995) Preservation of clay minerals in the Precambrian (1.1 Ga) Nonesuch Formation in the vicinity of the White Pine Copper Mine, Michigan. *Clays and Clay Minerals,* **43,** 361–376.

Merriman, R.J., Roberts, B., Peacor, D.R., and Hirons, S.R. (1995) Strain-related differences in the crystal growth of white mica and chlorite: a TEM and XRD study of the development of metapelitic microfabrics in the Southern Uplands thrust terrane, Scotland. *Journal of Metamorphic Geology,* **13,** 559–576.

Nicholson, S.W. and Shirey, S.B. (1990) Midcontinent rift volcanism in the Lake Superior region: Sr, Nd, and Pb isotopic evidence for a mantle plume origin. *Journal of Geophysical Research,* **95,** 10851–10868.

Nieto, F., Velilla, N., Peacor, D.R., and Huertas, M.O. (1994) Regional retrograde alteration of sub-greenschist faces chlorite to smectite. *Contributions to Mineralogy and Petrology,* **115,** 243–252.

Palmer, H.C. and Davis, D.W. (1987) Paleomagnetism and U-Pb geochronology of Michipicoten Island: Precise calibration of the Keweenawan polar wander track. *Precambrian Research,* **37,** 158–171.

Price, K.L. and McDowell, S.D. (1993) Illite/smectite geothermometry of the Proterozoic Oronto group, Midcontinent rift system. *Clays and Clay Minerals,* **41,** 134–147.

Price, K.L., Huntoon, J.E., and McDowell, S.D. (1996) Thermal history of the 1.1-Ga Nonesuch Formation, North American mid-continent rift, White Pine, Michigan. *American Association of Petroleum Geologists Bulletin,* **80,** 1–15.

Veblen, D.R., Guthrie, G.D., Jr, Livi, K.J.T., and Reynolds, R.C., Jr. (1990) High-resolution transmission electron microscopy and electron diffraction of mixed-layer illite/smectite: experimental results. *Clays and Clay Minerals,* **38,** 1–13.

Ziegler, K. and Longstaffe, F.J. (1997) Hydrogen isotopes from clay minerals and fluid flow along Precambrian/Cambrian unconformity in SW Ontario, Canada. In *Contributions to the Second International Conference on Fluid Evolution, Migration and Interaction in Sedimentary Basins and Orogenic Belts. Belfasts, Northern Ireland,* J.P. Hendry, P.F. Carey, J. Parnell, A.H. Ruffell, and R.H. Worden, eds., 343–346.

(Received 16 June 1997; accepted 12 June 1998; Ms. 97-054)